IOP Publishing Phys. Biol. 23 (2026) 016002 https://doi.org/10.1088/1478-3975/ae2c34

Physical Biology

PAPER

The interaction between dynamic ligand signaling and epigenetics in Notch-induced cancer metastasis

Tianchi Chen[1], **M Ali Al-Radhawi**[2], **Herbert Levine**[3,*] and **Eduardo D Sontag**[2,*]

[1] Department of Bioengineering, Northeastern University, Boston, MA, United States of America
[2] Departments of Electrical and Computer Engineering and Bioengineering, Northeastern University, Boston, MA, United States of America
[3] Departments of Physics and Bioengineering, and Center for Theoretical Biological Physics, Northeastern University, Boston, MA, United States of America
[*] Authors to whom any correspondence should be addressed.

E-mail: h.levine@northeastern.edu and e.sontag@northeastern.edu

Keywords: metastasis, melanoma, Notch signaling, miR-222, epigenetics

Supplementary material for this article is available online

OPEN ACCESS

RECEIVED
19 May 2025

REVISED
20 November 2025

ACCEPTED FOR PUBLICATION
12 December 2025

PUBLISHED
30 December 2025

Abstract

Metastatic melanoma presents a formidable challenge in oncology due to its high invasiveness and resistance to current treatments. Central to its ability to metastasize is the Notch signaling pathway, which, when activated through direct cell–cell interactions, propels cells into a metastatic state through mechanisms akin to the epithelial-mesenchymal transition (EMT). While the upregulation of miR-222 has been identified as a critical step in this metastatic progression, the mechanism through which this upregulation persists in the absence of active Notch signaling remains unclear. Here we introduce a dynamical system model that integrates miR-222 gene regulation with histone feedback mechanisms. Through computational analysis spanning both sustained and pulsatile ligand inputs, we delineate the non-linear decision boundaries that govern melanoma cell fate transitions, taking into account the dynamics of Notch signaling and the role of epigenetic modifications. Dimensional analysis reduces the 11-parameter system to three critical control groups governing chromatin modification rates and feedback strengths, providing a theoretical framework for parameter selection in the absence of complete kinetic measurements. Global sensitivity analysis identifies PRC2-mediated methylation and KDM5A-mediated demethylation as the dominant control parameters, while stochastic simulations show population heterogeneity consistent with the variable EMT responses observed in cancer cell populations. Our analysis examines the interplay between Notch signaling pathways and epigenetic regulation in dictating melanoma cell fate.

1. Introduction

Cancer metastasis represents a primary cause of mortality, with the epithelial-mesenchymal transition (EMT) playing a key role in conferring metastatic capabilities upon cancer cells [1–3]. The EMT, characterized by its reversibility, is modulated by a diverse array of environmental cues, EMT-inducing transcription factors (EMT-TFs), and epigenetic regulators [4, 5]. This research specifically targets melanoma, notable for its high resistance to treatment and propensity for metastasis.

The Notch signaling pathway is a critical player in development and disease, including metastasis [6–8]. It regulates cellular differentiation, proliferation, and fate determination [9]. In melanoma, Notch activation, for instance by keratinocytes expressing Notch ligands, can promote metastasis, partly through inhibition of the lineage survival oncogene MITF [10]. Conventionally, Notch activation requires direct cell-to-cell contact. However, melanoma cells can maintain a metastatic phenotype even after losing contact with ligand-expressing cells, suggesting a mechanism for persistence or memory [10].

A powerful approach to describe and resolve the complex interactions and feedback loops involved in genetic and epigenetic regulation is dynamical system modeling [11–13]. In particular, such methods

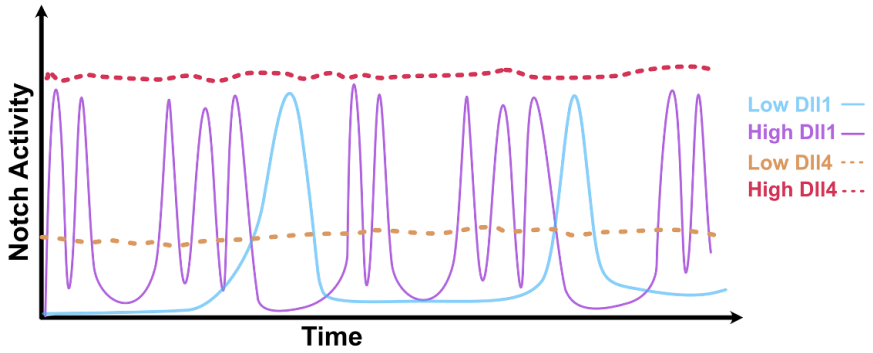

Figure 1. A conceptual view of distinct Notch signaling dynamics induced by DLL1-like and DLL4-like ligands. Experimental evidence suggests DLL1-like ligands can induce pulsatile NICD signals, In contrast, DLL4-like ligands tend to induce more sustained signals with an amplitude that increases with the concentration level of the ligand [20, 21]. The characteristics of these signals (amplitude, frequency, duration) can influence downstream cellular responses.

can be applied to regulatory mechanisms involving histone modifications such as H3K4me3 (activating) and H3K27me3 (repressive), which play an important role in EMT and cancer progression [14–16]. We propose that an epigenetic switching mechanism, involving feedback regulation of histone modifying enzymes, underlies the persistence of the Notch-induced metastatic state in melanoma. Specifically, we model the regulation of miR-222, whose expression is linked to melanoma metastasis [17] and influenced by Notch [10]. Our model incorporates the competition between NICD (the activated Notch intracellular domain) and MITF for the TF RBPJ, and links this competition to the recruitment of the H3K4me3 demethylase KDM5A [18], thereby influencing the histone state at the miR-222 locus. We hypothesize that positive feedback loops in the histone modification system create bistability, allowing the miR-222 locus to be switched to, and maintained in, an active state by a transient Notch signal. Computational analysis yields switching times within the experimentally observed EMT window [10, 19], with stochastic simulations (SI section 6) showing how intrinsic molecular noise generates population heterogeneity: the model predicts that only a fraction of cells undergo complete EMT under identical signaling conditions, reflecting the probabilistic nature of epigenetic state transitions.

Furthermore, different Notch ligands, such as DLL1-like and DLL4-like, can elicit distinct temporal dynamics of NICD activation—often pulsatile for DLL1-like and sustained for DLL4-like (figure 1) [20, 21]. These distinct dynamics can lead to differential activation of target genes [20]. A key question is how these dynamics are interpreted by downstream regulatory circuits. Our model investigates how the proposed epigenetic switch responds to both sustained (DLL4-like) and pulsatile (DLL1-like) NICD inputs, exploring whether the switch exhibits frequency-dependent filtering properties. We find that the epigenetic switch acts as a low-pass filter, which may place high-frequency DLL1-like signals at a relative disadvantage compared to sustained DLL4-like signals for initiating this specific epigenetic transition.

The manuscript is organized as follows. We introduce the computational model linking ligand-dependent NICD competition to miR-222 epigenetic regulation. We then analyze the model's bistable behavior and its response to sustained and pulsatile NICD signals, characterizing the switching boundaries (amplitude–frequency, A–ω, with A denoting signal amplitude and ω denoting signal frequency) and switching times (ST–ω, with ST denoting the switching time). We investigate how altering epigenetic parameters, particularly PRC2 feedback strength, reshapes these response characteristics. Finally, we discuss the implications of the model for dynamic signal processing, epigenetic memory, and therapeutic relevance. SI sections 2–6 provide the extended analyses, including the nondimensional formulation, sensitivity and Monte Carlo screens, waveform robustness tests, solver benchmarking, and stochastic pulse-counting simulations.

2. Methods

2.1. Model description

Our model (figure 2) integrates Notch signaling input with epigenetic regulation of miR-222. It consists of two coupled modules.

Module 1: NICD-MITF competition. Upon Notch receptor activation by a ligand, the notch intracellular domain (NICD, denoted N) is released and translocates to the nucleus, where it undergoes rapid turnover through proteasomal degradation on the timescale of hours [22, 23]. There, it competes with

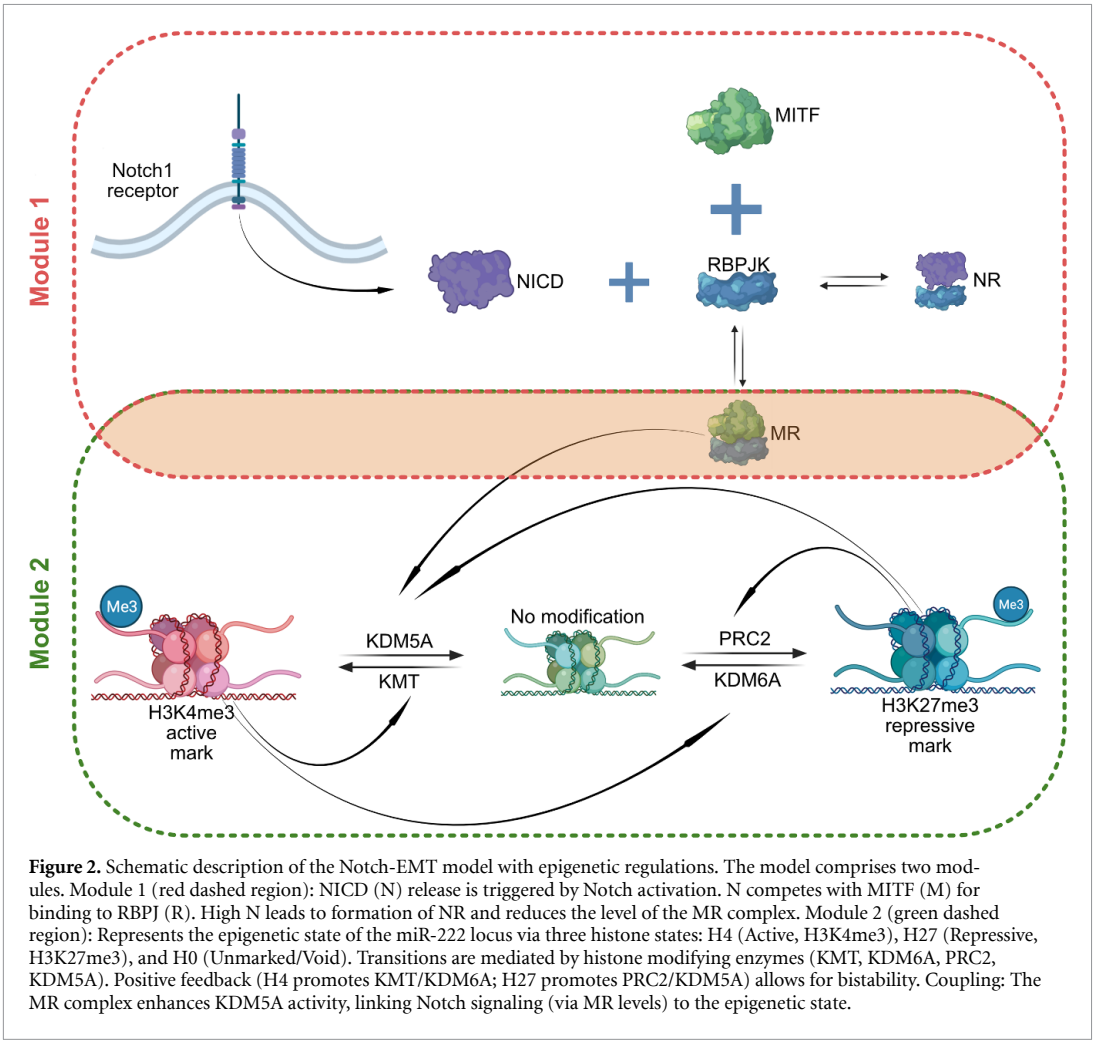

Figure 2. Schematic description of the Notch-EMT model with epigenetic regulations. The model comprises two modules. Module 1 (red dashed region): NICD (N) release is triggered by Notch activation. N competes with MITF (M) for binding to RBPJ (R). High N leads to formation of NR and reduces the level of the MR complex. Module 2 (green dashed region): Represents the epigenetic state of the miR-222 locus via three histone states: H4 (Active, H3K4me3), H27 (Repressive, H3K27me3), and H0 (Unmarked/Void). Transitions are mediated by histone modifying enzymes (KMT, KDM6A, PRC2, KDM5A). Positive feedback (H4 promotes KMT/KDM6A; H27 promotes PRC2/KDM5A) allows for bistability. Coupling: The MR complex enhances KDM5A activity, linking Notch signaling (via MR levels) to the epigenetic state.

the TF MITF (M) for binding to the DNA-binding protein RBPJ (R). In the absence of NICD, MITF binds RBPJ to form the MR complex. When NICD is present, it binds RBPJ to form the NR complex, thereby reducing the amount of available R and consequently reducing the concentration of the MR complex. The production rate of N, denoted 'Signal(t)', represents the strength and dynamics of the external Notch ligand stimulus.

Module 2: Epigenetic regulation of miR-222. We model the histone state associated with the miR-222 gene locus using three states: H4 (representing an active state, high H3K4me3), H27 (representing a repressed state, high H3K27me3), and H0. The H0 state represents an unmarked or intermediate chromatin configuration. In our model, this state is assumed to correspond to a basal or low level of miR-222 transcription, distinct from the actively repressed H27 state (low/off miR-222) and the highly active H4 state (high miR-222). It primarily serves as a transient state through which the locus passes during switching between the H4 and H27 states. The transitions between these states are governed by the activity of four types of histone modifying enzymes: KMTs (adding H3K4me3), KDM6A (removing H3K27me3), PRC2 (adding H3K27me3), and KDM5A (removing H3K4me3). Crucially, the model includes positive feedback loops: the H4 state promotes the production/activity of KMT and KDM6A, while the H27 state promotes the production/activity of PRC2 and KDM5A. This double-positive feedback structure can generate bistability between the H4-high and H27-high states.

Module coupling. The two modules are linked via the MR complex. Based on experimental findings [10, 18], we assume that the MR complex enhances the production or recruitment of the H3K4me3 demethylase KDM5A to the miR-222 locus. Therefore, high MITF activity (high MR, low NICD) promotes the H27 state (miR-222 repression), while high Notch activity (low MR, high NICD) disinhibits KDM5A recruitment, allowing the feedback loops to potentially switch the system to the H4 state (miR-222 activation).

Table 1. CRN model of the Notch-miR222 circuit. Module 1 is driven by input NICD (N) concentration (Signal(t)) and reflects the NICD competition with MITF (M) for RBPJ (R). Module 2 describes the epigenetic regulation of histone states (H4, H0, H27) via enzymes (KDM5A, KDM6A, PRC2, KMT), including feedback loops and basal production/degradation. The modules are coupled via MR-enhanced KDM5A production/recruitment (rate k_0).

NICD, MITF competition (R1-R2)	$R \underset{k_3}{\overset{\text{Signal}(t)}{\rightleftharpoons}} NR$ $M + R \underset{k_2}{\overset{k_1}{\rightleftharpoons}} MR$
Core histone regulation (Module 2)	$H4 + KDM5A \xrightarrow{d} H_0 + KDM5A$ $H0 + PRC2 \xrightarrow{m} H27 + PRC2$ $H27 + KDM6A \xrightarrow{d1} H0 + KDM6A$ $H0 + KMT \xrightarrow{m1} H4 + KMT$
Epigenetic feedback (Module 2)	$MR \xrightarrow{k_0} MR + KDM5A$ (MR induction of KDM5A) $H27 \xrightarrow{p} H27 + PRC2$ (H27 feedback on PRC2) $H4 \xrightarrow{kk} H4 + KDM6A$ (H4 feedback on KDM6A) $H4 \xrightarrow{pp} H4 + KMT$ (H4 feedback on KMT) $H27 \xrightarrow{k} H27 + KDM5A$ (H27 feedback on KDM5A)
Enzyme Production (Module 2)	$\varnothing \xrightarrow{\alpha_1} KDM6A$ $\varnothing \xrightarrow{\alpha_1} KMT$ $\varnothing \xrightarrow{\alpha_1} PRC2$ $\varnothing \xrightarrow{\alpha_1} KDM5A$ (Basal production)
Enzyme Degradation (Module 2)	$PRC2 \xrightarrow{\delta} \varnothing$ $KDM5A \xrightarrow{\delta} \varnothing$ $KDM6A \xrightarrow{\delta} \varnothing$ $KMT \xrightarrow{\delta} \varnothing$

Mathematical model

We formulated the model using chemical reaction networks (CRNs) [24], assuming mass-action kinetics (table 1).

State variables are the concentrations of the molecules listed in table 2.

Parameters. table 3 lists the parameter sets used throughout the manuscript. Set A underpins figures 3 and 4, whereas Set B represents the higher-feedback regime employed for the PRC2 modulation sweep in figure 5. These sets follow from the non-dimensional analysis and parameter sweeps detailed under 'Parameter Estimation Methodology' in section 2, ensuring bistable switching, realistic timescales, and experimentally motivated ligand responses. Unless otherwise noted, simulations adopt these values together with the ligand input definitions given later in section 2.

Modeling time-varying signals

To simplify our analysis, we model time-varying pulsatile signals by square waves. On the other hand, it has been observed experimentally that Notch signaling often exhibits exponential NICD decay with measured half-lives of 2–4 h following ligand binding [20, 22, 23]. Thus, in order to assess model robustness to waveform shape, we implemented exponential decay signals with time constants $\tau = 2$, 5, and 10 h and systematically explored the amplitude–frequency parameter space (SI section 4, figure S4). Exponential pulses require 4–8 fold higher amplitudes than square waves to achieve switching (e.g. $\tau = 2$ h pulses need $\geqslant$400 nM versus 50 nM for square waves at equivalent frequency). The non-monotonic frequency-amplitude boundary persists across waveforms, with efficient switching occurring when signal frequency matches chromatin timescales ($\omega \approx 1/\tau_c$). These results confirm frequency-dependent signal integration as an intrinsic property of chromatin feedback architecture. We retain square pulses in the main text for clarity while demonstrating waveform robustness in the SI.

Units and plotting conventions

Time is reported in hours, ω in h^{-1}, and kinetic rates in h^{-1} unless specified. Concentrations are normalized (a.u.) and consistent across figures. All axes include units in labels, and all figures use the Wong colorblind-safe palette [25] with consistent line styles for accessibility.

Table 2. State variables of the CRN model.

State Variable	Description
R	Free RBPJ concentration.
NR	RBPJ bound to NICD complex concentration.
M	Free MITF concentration.
MR	MITF-RBPJ complex concentration.
H4	Concentration of loci in the 'Active' histone state (high H3K4me3).
H0	Concentration of loci in the 'Unmarked/Void' histone state.
H27	Concentration of loci in the 'Repressive' histone state (high H3K27me3).
KDM5A	H3K4me3 demethylase concentration.
KDM6A	H3K27me3 demethylase concentration.
PRC2	H3K27me3 methyltransferase concentration.
KMT	H3K4me3 methyltransferase concentration.

Table 3. Parameters of the CRN model and default values used. Total amounts of M, R, and histone sites (H0+H4+H27) are conserved or implicitly set. Set A drives the sustained/pulsatile trajectories and A–ω sweeps; Set B underlies the PRC2 modulation sweep. Entries marked with [a] were varied in the Sobol global sensitivity analysis (SI section 3). The parameter values emerge from systematic dimensional analysis (SI section 2) that reduces the 11-parameter model to three control groups governing bistable switching: $\Pi_2 = d \cdot \tau_c \cdot E_c/H_c$ (H3K4me3 demethylation timescale), $\Pi_3 = m \cdot \tau_c \cdot E_c/H_c$ (H3K27me3 methylation timescale), and $\Pi_4 = pp/kk$ (feedback strength ratio). Set A yields $\Pi_2 \approx 1.0$, $\Pi_3 \approx 2.0$, $\Pi_4 = 6.0$, positioning the system on the mesenchymal-favoring side of the bistable manifold; Set B yields $\Pi_2 \approx 3.9$, $\Pi_3 \approx 2.0$, $\Pi_4 = 1.0$, representing a higher-demethylation, balanced-feedback regime for PRC2 modulation studies. Both sets were selected from 2252 validated bistable configurations (47% of 4800 tested combinations) to maintain EMT transition timescales on the order of hours to days, consistent with melanoma progression [10, 19]. The characteristic scales used are $\tau_c = 24$ h (representative day-scale EMT timescale) and $E_c/H_c = 0.2$ (typical enzyme-to-histone stoichiometry).

Parameter	Value (Set A: figures 3 and 4)	Value (Set B: figure 5)	Description
A	Varies	Varies	NICD signal amplitude
ω	Varies	Varies	NICD pulse frequency
ϕ	Varies	Varies	NICD pulse phase
k_3	1.0	1.0	NR dissociation rate (normalized)
k_1	1.0	1.0	M-R binding rate
k_2	1.0	1.0	MR unbinding rate
k_0	1.0	1.0	MR-driven KDM5A recruitment
d[a]	0.21	0.81	KDM5A-mediated H4 demethylation
d_1	1.0	1.0	KDM6A-mediated H27 demethylation
m[a]	0.41	0.41	PRC2-mediated H0 $\rightarrow$ H27 methylation
m_1	1.0	1.0	KMT-mediated H0 $\rightarrow$ H4 methylation
p	6.0	16.0	H27-enhanced PRC2 production
k	0.0	0.0	H27-enhanced KDM5A production
pp[a]	6.0	11.0	H4-enhanced KMT production
kk[a]	1.0	11.0	H4-enhanced KDM6A production
α_1	1.0	1.0	Basal enzyme production rate
δ	1.0	1.0	Enzyme degradation rate

[a] Parameters varied in the Sobol global sensitivity analysis (SI section 3).

Ordinary differential equations (ODEs)

The corresponding **ODEs** derived from table 1 assuming mass-action kinetics are:

$$\frac{\mathrm{d}[R]}{\mathrm{d}t} = -\mathrm{Signal}(t)\cdot[R] + k_3[NR] - k_1[M][R] + k_2[MR], \quad (1)$$

$$\frac{\mathrm{d}[NR]}{\mathrm{d}t} = \mathrm{Signal}(t)\cdot[R] - k_3[NR], \quad (2)$$

$$\frac{\mathrm{d}[M]}{\mathrm{d}t} = -k_1[M][R] + k_2[MR], \quad (3)$$

$$\frac{\mathrm{d}[MR]}{\mathrm{d}t} = k_1[M][R] - k_2[MR], \quad (4)$$

$$\frac{\mathrm{d}[KDM5A]}{\mathrm{d}t} = \alpha_1 + k_0[MR] + k[H27] - \delta[KDM5A], \quad (5)$$

$$\frac{\mathrm{d}[H4]}{\mathrm{d}t} = -d[H4][KDM5A] + m_1[H0][KMT], \quad (6)$$

$$\frac{\mathrm{d}[H0]}{\mathrm{d}t} = d[H4][KDM5A] - m[H0][PRC2] + d_1[H27][KDM6A] - m_1[H0][KMT], \quad (7)$$

$$\frac{\mathrm{d}[PRC2]}{\mathrm{d}t} = \alpha_1 + p[H27] - \delta[PRC2], \quad (8)$$

$$\frac{\mathrm{d}[H27]}{\mathrm{d}t} = m[H0][PRC2] - d_1[H27][KDM6A], \quad (9)$$

$$\frac{\mathrm{d}[KDM6A]}{\mathrm{d}t} = \alpha_1 + kk[H4] - \delta[KDM6A], \quad (10)$$

$$\frac{\mathrm{d}[KMT]}{\mathrm{d}t} = \alpha_1 + pp[H4] - \delta[KMT]. \quad (11)$$

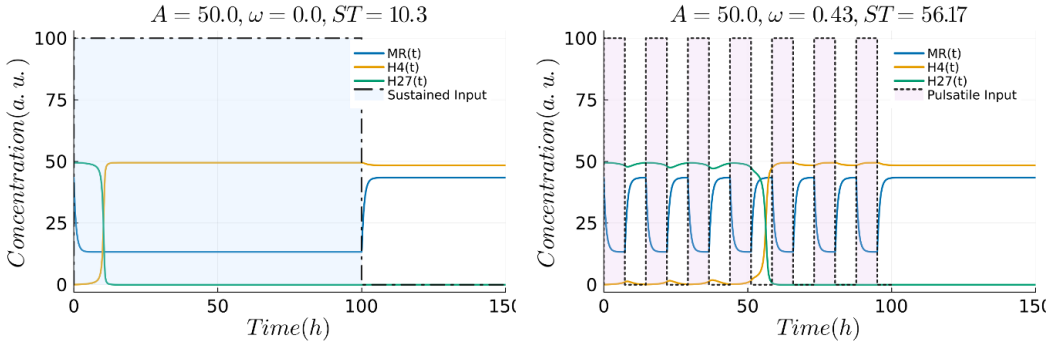

(a) Sustained DLL4-like signal (b) Pulsatile DLL1-like signal

Figure 3. Both sustained (DLL4-like) and pulsatile (DLL1-like) NICD dynamics can induce persistent switching of the miR-222-associated histone state. Simulations start from the H27-high state (blue). Signal is applied from $T = 0$ to $T = 100$ ($\Delta T = 100$). Panel (a) uses a sustained input ($Signal(t) = A = 50$) that triggers a switch to the H4-high state (red), which persists after signal removal; panel (b) shows a pulsatile input ($SLignal(t) = 50 \times [1 + \text{sign}(\cos(0.43\,t))]/2$, $\phi = 0$) that also drives persistent switching. Units: time (h), concentration (a.u.).

Conservation laws hold for total RBPJ ($R_{\text{tot}} = [R] + [NR] + [MR]$), total M ($M_{\text{tot}} = [M] + [MR]$), and all possible Histone modifications ($H_{\text{tot}} = [H0] + [H4] + [H27]$).

Region of bistability

A key goal of this model is to explain the observed persistence of the metastatic phenotype even after the initiating Notch signal is removed [10]. We hypothesize that this persistence arises from epigenetic memory, mechanistically represented in the model by bistability within the epigenetic module (Module 2). This bistability allows the system to switch between two stable steady states—one corresponding to low miR-222 expression (i.e. H27-high) and another to high miR-222 expression (H4-high)—and remain in the new state after a transient input.

The existence of bistability is fundamental to the model's ability to exhibit epigenetic memory. We employed standard numerical methods for finding steady states and performing linear stability analysis (based on the eigenvalues of the Jacobian matrix) to identify parameter regimes, including the default set in table 3, that support this behavior. For these parameters and in the absence of Notch input (`N = 0`), the analysis confirmed that the system exhibits exactly two stable steady states: one corresponding to the repressed state (high H27, low H4) and one corresponding to the active state (high H4, low H27). An unstable steady state typically exists between them. Other potential configurations, such as states dominated by H0, were found to be unstable within the parameter regime supporting bistability between the primary H4-high and H27-high states. In principle it would be possible to search for parameter sets for which the model exhibits tri-stability, but these systems would not be relevant for the biological phenomena we are attempting to capture.

The bistability itself emerges from the positive feedback loops inherent in the epigenetic regulation: the H4 state promoting enzymes for its own maintenance (KMT, KDM6A) and the H27 state similarly promoting its maintenance factors (PRC2, KDM5A), as detailed in table 1. The existence and parameter range of this bistability critically depend on the strengths of these feedback loops and the rates of histone modification (k_0, d, m, p, k, pp, kk, etc). Therefore, identifying parameter sets that permit bistability is essential for the model to capture the desired memory behavior. We utilized numerical continuation techniques, specifically Homotopy Continuation [26], to explore the parameter space and identify regimes, such as the default parameters listed in table 3, that yield the necessary two stable steady states in the absence or presence of low Notch input ('Signal(t)' close to 0).

Numerical verification of bistability

methods. The existence of exactly two stable steady states was verified through systematic numerical analysis: (i) Homotopy continuation methods were applied across the parameter database (20 random initial conditions per parameter set, yielding 2252 bistable sets from 4800 evaluated combinations) with equilibria filtered by eigenvalue stability criteria; (ii) Basin-of-attraction analysis using 20×20 grids of initial conditions confirmed that trajectories converge exclusively to one of two stable equilibria (integration performed using Rosenbrock23, absolute tolerance $= 10^{-9}$, relative tolerance $= 10^{-8}$); (iii) Long-horizon simulations under both zero and sustained Notch signals demonstrated convergence to the same two equilibria without evidence of additional stable states. All equilibrium candidates beyond the two stable nodes exhibited positive real eigenvalues, confirming their instability. Complete methodology and numerical results are presented in SI section S1.

ODEs were solved numerically using standard solvers available in Julia programming language packages. Simulations typically started from the H27-high steady state (representing the non-metastatic state). Notch input signals ('Signal(t)') were applied for a duration ΔT (ranging from 50 to 100 time units depending on the specific analysis), and the system's evolution was monitored. Switching time (ST) was defined as the time required for the H4 state concentration to cross a predefined threshold (e.g. half its maximum value in the H4-high state) after the signal onset.

2.2. Algorithms and parameters

The specific parameter values used for simulations are listed in table 3, unless otherwise stated. These values were selected, using the numerical methods described under 'Region of bistability', primarily to ensure the model exhibits bistability within the epigenetic module (Module 2). This feature is key for representing epigenetic memory based on the positive feedback structure described. While not directly fitted to quantitative experimental data for this specific miR-222 regulatory system in melanoma, the chosen values represent plausible relative strengths and timescales for feedback-driven epigenetic processes often observed in biological circuits [27–30].

Concentrations and kinetic parameters are given in arbitrary units (a.u.). Also, note that our parameter choices establish relative reaction rates that yield the reported dynamics, such as switching events. Experimentally, these events occur on timescales ranging from hours to days, consistent with typical epigenetic processes [31, 32]. This sets an approximate value of our time unit as several hours, but a more direct mapping to real time would require calibration via comparison with a specific experimental dataset.

Parameter estimation methodology

Given the absence of complete kinetic measurements for the Notch-epigenetic system in melanoma, we employed a phenomenological modeling approach [33] anchored in the dimensionless formulation developed in SI section 2. Our comprehensive literature survey revealed that none of the 11 model parameters are directly measured from melanoma EMT experiments—only KDM5A activity can be indirectly constrained through H3K4me3 half-life measurements ($t_{1/2} = 6.8$ h). Rather than attempting ill-posed parameter fitting to sparse endpoint data, we adopt a theoretical framework where parameters are chosen to reproduce qualitative hallmarks of melanoma EMT: transitions occurring over hours to days [10, 19], bistable epithelial/mesenchymal states, and requirement for sustained or repeated Notch activation. The non-dimensionalization collapses the dynamics onto a handful of Π-groups (e.g. $\Pi_2 = d\,\tau_c(E_c/H_c)$, $\Pi_3 = m\,\tau_c(E_c/H_c)$, $\Pi_4 = pp/kk$) that highlight the dominant ratios of histone modification rates and feedback strengths. We therefore selected dimensional parameters by: (i) fixing the characteristic time-scale $\tau_c =$ 24 h to represent the day-scale EMT transition timescale, chosen to match the general observation that melanoma EMT occurs over hours to days [10, 19]; (ii) seeding rate constants so that the associated Π-groups fall near $\mathcal{O}(1)$, which corresponds to balanced methylation/demethylation fluxes; and (iii) sweeping the remaining degrees of freedom around these nominal values to ensure bistability, realistic switching times, and pulse integration consistent with DLL1-like/DLL4-like experiments [20, 21]. In total we evaluated 4800 parameter combinations (2252 of which exhibited the desired bistable manifold), from which the Set A and Set B values in table 3 were drawn.

We performed a global sensitivity analysis (Sobol variance decomposition) over biologically plausible parameter ranges [34]; detailed sampling results appear in the Results section and SI section 3.

The external Notch input is represented by 'Signal(t)' in the ODEs (equations 1-2), modeling the effective concentration of NICD generated. To simulate different ligand inputs observed experimentally [20, 21], we consider the following two scenarios:

- **Sustained (DLL4-like) input:** we use a constant signal, $Signal(t) = A$, during the stimulation period.
- **Pulsatile (DLL1-like) input:** we use a square wave oscillating between 0 and amplitude A, represented as $Signal(t) = A \times [1 + \mathrm{sign}(\cos(\omega t + \phi))]/2$, during stimulation. Here, A is the amplitude, ω is the frequency, and ϕ is the initial phase. This form captures the essential on/off nature of pulsatile signaling.

Numerical integration. Simulations were performed in Julia (v1.8+) using `DifferentialEquations.jl`. The reaction network—encoded with `Catalyst.jl`—was integrated by the stiff solver `Rosenbrock23` (abs./rel. tolerances 10^{-6}). Trajectories were initialized in the H27-high steady state, followed by a stimulus of duration ΔT (50–100 a.u.). The total runtime was $t_{\max} = 1.5\,\Delta T$.

Switching criterion. A switch is said to occur when the active-mark species H4 first exceeds the repressive mark H27. Internally, a helper routine scans the numerical solution and returns the first crossing time, denoted ST; if no crossing occurs, the run is classified as non-switching.

Phase-independent boundary construction. The DLL1-like input is modeled as a square wave $Signal(t) = A\left[1 + \mathrm{signcos}(\omega t + \phi)\right]/2$. For every non-zero driving frequency ω we set the initial phase to $\phi^* = \frac{3\pi}{2}$, so that $Signal(t) = 0$ for $t < 0$ and the

first positive half-cycle starts exactly at the simulation onset $t = 0$. Because any other choice of ϕ shifts the waveform leftward in time, ϕ^* produces the *latest* possible arrival of the first activating pulse and therefore represents the mathematically 'worst-case' phase for switching.

We then sweep the control parameters over $A \in [0, 300]$ with unit resolution and $\omega \in [0, 2]$ with step 0.02. For each ω we record the smallest amplitude that leads to a switch—this is the conservative threshold $A^*(\omega)$. Connecting the points $\{(\omega, A^*)\}$ yields the phase-independent amplitude–frequency decision boundary shown in figure 4(a). It is important to note that this decision boundary, and the corresponding switching times presented in figure 4(b), were specifically computed for a fixed stimulus duration of $\Delta T = 100$ a.u. These boundaries can be dependent on the total stimulus duration; longer durations might allow for switching with weaker or higher-frequency pulsatile signals due to cumulative effects over more cycles, a characteristic not explicitly explored in the current boundary plots. However, further analysis demonstrates that this dependency is weak; for example, increasing the total stimulus duration from $\Delta T = 100$ a.u. to $\Delta T = 200$ a.u. results in a slight leftward shift of the A-ω boundary. Specifically, at a driving frequency of $\omega = 1.0$, the minimum amplitude required for switching decreases from approximately $A = 185$ (for $\Delta T = 100$ a.u.) to $A = 180$ (for $\Delta T = 200$ a.u.). This demonstrates that the system can switch with a slightly weaker signal if the stimulation is applied for a longer total period, confirming the cumulative effect of pulsatile signals over extended durations.

The same simulations provide the switching time $ST(A, \omega, \phi^*)$, defined as the first instant at which the active mark H4 exceeds the repressive mark H27. Grouping these values by amplitude produces the ST–ω curves in figure 4(b); each curve is an upper envelope valid for all initial phases, because any $\phi \neq \phi^*$ can only advance the first pulse and shorten the observed switching time.

Validation of phase independence. For representative (A, ω) pairs we repeated the simulations while sampling ϕ uniformly in $[0, 2\pi)$. The maximal switching time and the minimal switching amplitude obtained over the full phase ensemble coincided (within numerical tolerance) with $ST(A, \omega, \phi^*)$ and $A^*(\omega)$, respectively, confirming that the reported boundary and ST curves are indeed independent of the initial phase.

3. Results

The CRN model presented in table 1 provides a framework for understanding the dynamics of Notch signaling activation and its influence on the histone state of miR-222. In a previous study [10], researchers observed that melanoma cells could maintain Notch pathway activation and a metastatic phenotype even when not in direct contact with ligand-expressing keratinocytes. This persistence suggests an underlying memory mechanism. The surface of sender cells contains DLL1-like and DLL4-like ligands, which trigger distinct signaling patterns when Notch is activated: pulsatile signaling is often associated with DLL1-like inputs, and sustained signaling with DLL4-like [20, 21]. However, the relationship between the dynamics of Notch signaling in melanoma metastasis and its epigenetic impact on miR-222 remained unexplored.

3.1. Notch ligand dynamics determines melanoma cell state transition

In this paper, we focus primarily on the histone state of the miR-222 gene as an indicator of the metastatic melanoma phenotype. We systematically explore the transition between epigenetic states by studying the switching time (ST) of the histone state in the presence of both sustained (DLL4-like) and frequency-modulated pulsatile (DLL1-like) Notch signals. Experimental evidence has shown that induced dynamics of NICD by different Notch ligands can lead to different activation patterns of downstream Notch-targeted genes, which in turn determine cell fate [20]. In the following results, we analyze how ligand dynamics and epigenetic mechanisms coordinate epigenetic state transitions in our model.

3.1.1. DLL4-like ligand-induced sustained NICD triggers persistent melanoma metastasis

While the molecular interactions are believed known, the precise dynamical mechanism establishing persistent cellular memory via Notch signaling requires further elucidation. We initially simulated the model using a sustained DLL4-like Notch ligand signal as the external input ($Signal(t) = A$). The simulation results qualitatively reproduced the experimental observations of phenotypic persistence [10]. We used a default set of model parameters (given in table 3) that allowed for bistable histone states and initialized the model from a repressed histone state (H27-high). This setup mimics the experimental finding of high-level repressive histone marks in melanoma in a Notch-free environment [10]. Our model assumes that miR-222 is maintained in a repressed state due to MR-mediated KDM5A activity and the double-positive feedback in the histone methylation circuit. Upon activation of the Notch signaling pathway with sufficient amplitude and duration, the histone state is expected to switch from a repressive state to an activated state.

Figure 3(a) presents an example simulation illustrating how a sustained DLL4-like Notch ligand signal ($A = 50$ applied from $T = 0$ to $T = 100$, so $\Delta T = 100$) induces an epigenetic state change for miR-222, potentially leading to an invasive and metastatic state. The histone state of miR-222 is initially

repressed (high H27) and then transitions to the active state (high H4) while the signal is active. At $T = 100$, the Notch ligand signal is removed. The simulation demonstrates that the histone state of miR-222 remains in the active state, consistent with experimental observations of persistence. Our simulation results suggest that the model provides a plausible framework at the epigenetic level for explaining the persistence of a high miR-222 state (associated with invasive melanoma cells even after the removal of the Notch signal.

3.1.2. DLL1-like ligand-induced pulsatile NICD can also trigger persistent metastatic melanoma states

The activation of the Notch signaling pathway by DLL1-like and DLL4-like ligands leads to distinct NICD dynamics (figure 1). Emerging studies demonstrate the differential effects of DLL1-like and DLL4-like [20, 35, 36]. This specificity is partly attributed to ligand-receptor interactions modulating these NICD dynamics [20].

So far, we have shown that the DLL4-like ligand can induce a stable change in histone configuration, ultimately leading to the activation of miR-222 (figure 3(a)). To understand the influence of DLL1-like ligand input, we modeled pulsatile NICD signals using the square wave form $Signal(t) = A \times [1 + \text{sign}(\cos(\omega t + \phi))]/2$ during stimulation. The simulation results, depicted in figure 3(b), reveal that pulsatile induction through DLL1-like signals is also capable of initiating and sustaining miR-222 activation over an extended period, similar to the sustained input from DLL4-like ligands, given appropriate parameters. The mechanism underlying this response to pulses involves signal integration over time. The epigenetic modification system (Module 2) operates on timescales slower than the NICD fluctuations driven by the pulsatile input. Consequently, while a single short pulse (like the first pulse in figure 3(b), shorter than the switching time seen in figure 3(a)) is typically insufficient to cause an irreversible switch, its effect (reducing MR and allowing H4 mark accumulation) partially persists through the 'off' phase. Subsequent pulses build upon this lingering effect. If the pulses are sufficiently frequent and sustained over time, the cumulative impact drives the histone state across the threshold for activation, and thereafter the internal positive feedback loops can maintain the H4-high state after the signal ends.

Thus, our analysis confirms that both sustained and pulsatile NICD dynamics can induce long-lasting epigenetic changes, leading to stable high-H4 (active miR-222) melanoma cell states, consistent with experimental observations of persistence [10]. Histone transitions triggered by DLL1-like-induced pulsatile NICD dynamics ultimately exhibit a persistent final pattern similar to that induced by sustained dynamics. However, as discussed further in the context of frequency-dependence in the next section, the efficiency of this integration process is sensitive to the pulse characteristics (amplitude, frequency, duration). Excessively rapid pulsatile NICD dynamics can hinder the system's ability to react within each short signaling window, subsequently stalling the transition; this can be thought of as low-pass filtering. Mechanistically, our simulations reveal that the epigenetic system counts discrete signal pulses: cells require multiple pulses to accumulate sufficient chromatin modifications for irreversible switching, with the exact number determined by frequency and amplitude (SI section 4). At low frequencies (0.2–0.3 h^{-1}), fewer but longer pulses enable cumulative H3K4me3 deposition across each cycle; at high frequencies (0.8–1.0 h^{-1}), rapid pulsing maintains elevated baseline enzyme activity by preventing complete NICD degradation between pulses. This pulse-counting mechanism, verified through both deterministic parameter sweeps and stochastic simulations (SI Sections 4, 6), explains why intermediate frequencies (0.4–0.6 h^{-1}) are inefficient: they neither allow sufficient per-pulse modification nor maintain steady enzyme levels.

3.2. Decision boundary of melanoma cell state transition

We mapped how sustained (DLL4-like) and pulsatile (DLL1-like) Notch ligands define the amplitude–frequency combinations required for chromatin switching. Sustained signals drive transitions through continuous NICD input, while pulsatile signals require specific temporal patterns matching chromatin timescales. To understand how signal characteristics influence this switch, we computationally determined transition boundaries (minimum amplitude A for switching vs. frequency ω) as well as the switching times ST as a function of (A, ω). This analysis aims to clarify how the intrinsic properties of ligand signals collectively influence the thresholds for cell state transitions and the timescale of commitment.

An important aspect of pulsatile signaling is the initial phase (ϕ) of the signal. In the computational model, the initial phase affects only the duration of the first pulse, with subsequent pulses being unaffected. This dependence can influence the minimum number of pulses needed to cause a transition. Biologically, this phase must represent the (in general fluctuating) state of the cell at the onset of signal receipt. This initial alignment is likely to be random from cell to cell. To capture the most robust system behavior, one can analyze phase-independent behavior. A phase-independent amplitude threshold (for the A–ω curve) represents the minimum amplitude required to guarantee switching regardless of the phase, determined by the 'worst-case' phase. Similarly, a phase-independent switching time (for the ST–ω curve) represents the maximum time required to switch across all possible phases.

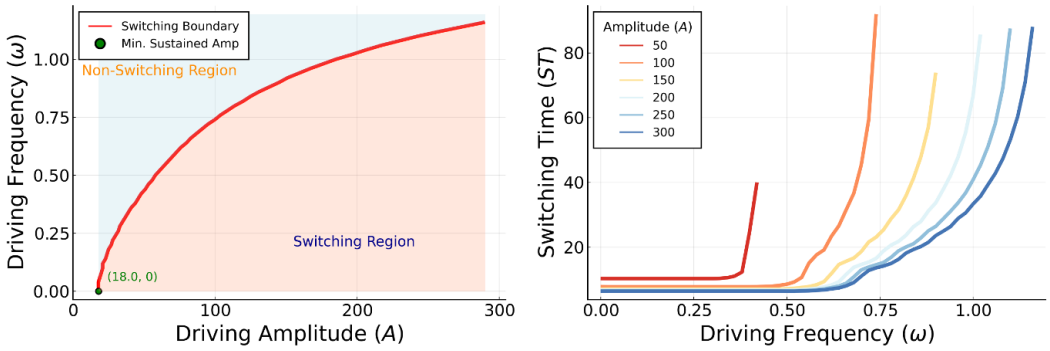

(a) Amplitude–frequency boundary (b) Switching-time boundary

Figure 4. Dependence of epigenetic switching on NICD signal dynamics (phase-independent boundaries computed for duration $\Delta T = 50$). Panel (a) shows the amplitude–frequency (A–ω) switching boundary: minimum amplitude A (a.u.) required to ensure switching versus frequency ω (h^{-1}), regardless of initial phase ϕ. Higher frequencies require larger amplitudes, reflecting low-pass filtering. Panel (b) reports the switching time–frequency (ST–ω) relation: maximum switching time ST (h) (over all phases ϕ) versus frequency ω (h^{-1}) for fixed amplitudes ($A = 50, 100, 200, 300$; a.u.). ST increases sharply above a characteristic frequency for each amplitude; minor undulations reflect discrete pulse counting and phase effects rather than numerical artifacts.

3.2.1. Amplitude and frequency effects

Figure 4(a) displays the phase-independent A–ω switching boundary curve. This curve maps out the minimum NICD signaling amplitude (A) required to ensure that a stable histone switch occurs at a specific frequency (ω) within a fixed duration ($\Delta T = 50$), regardless of the initial signal phase ϕ. It reveals a nonlinear relationship: at low frequencies, a certain minimum amplitude is needed, while at higher frequencies, a larger amplitude is required to achieve switching. This confirms the low-pass filtering nature of the epigenetic switch—it responds less efficiently to high-frequency inputs. This phase-independent threshold reflects the robust signaling strength required to guarantee the epigenetic transition.

3.2.2. Switching time—frequency (ST–ω) relation

Building upon the A–ω relationship, figure 4(b) illustrates the phase-independent ST–ω relationship, showing the maximum switching time (ST_{max}) observed across all initial phases ϕ as a function of frequency (ω) for several fixed amplitudes (A). This represents the 'worst-case duration' required for a histone state to shift. Analysis shows that this worst-case duration increases with frequency (ω) above a certain threshold, reflecting low-pass filtering. For the canonical parameters (table 3), our simulations predict switching times of 12–16 h at low signal frequencies ($\omega \approx 0.2$-$0.3\ h^{-1}$) to over 45 h at high frequencies, timescales on the order of hours to days typical of EMT processes. Notably, when the frequency is zero ($\omega = 0$), the ST aligns with what is expected for a sustained DLL4-like signal as phase is clearly irrelevant for a constant signal.

More detailed scrutiny of the ST–ω data reveals that while pulsatile signals from DLL1-like ligands may induce epigenetic changes, they are never faster (especially considering the worst-case phase) than DLL4-like sustained signals in terms of hastening histone state transition times (compare ST_{max} at $\omega = 0$ versus $\omega > 0$ for a given A). Moreover, the findings underscored in figure 4(b) convey that at each fixed amplitude, starting from zero frequency, the maximum switching time remains constant up until a definable frequency threshold. Beyond this juncture, the maximum switching time begins increasing rapidly with frequency and eventually diverging at the transition boundary. In essence, the A–ω and ST-ω curves reveal how both sustained and dynamic ligand signals can facilitate these epigenetic transitions, albeit within specific parameter ranges. Empirically, this variation in response likely contributes to observations wherein different dynamic signals initiate disparate sets of downstream target [20]. We note that small undulations apparent in figure 4(b) arise from discrete pulse-counting and phase effects near threshold, not numerical instability; results are invariant to integrator choice and tolerance (see SI).

3.3. Cooperative control of cell fate by epigenetics and ligand dynamics

Our in-depth examination of the miR-222 gene model has provided key insights into how dynamic ligand signals interact with epigenetic regulation to drive state transitions potentially relevant to EMT in melanoma. Within this framework, histone methylation mediated by PRC2 serves as a key epigenetic control mechanism stabilizing the repressed state. Understanding how PRC2 kinetics influence cell fate transitions provides deeper insight into the coordinated effects of Notch ligand signaling and epigenetic feedback in melanoma progression [37–40].

3.3.1. Epigenetics and ligand dynamics jointly steer cell fate determination

To gain deeper insight into how PRC2 rate modulates cell fate decisions, we investigate its role in regulating the threshold at which NICD signaling induces miR-222 activation. The precise timing and strength of Notch ligand signals, coupled with epigenetic repression mechanisms, determine whether a melanoma cell switches its epigenetic state.

The PRC2 complex is a crucial histone methyltransferase that catalyzes the deposition of H3K27me3 [41]. Thus, changes in PRC2 rate via parameter p) affect the stability of the repressive histone state and alter the Notch signaling threshold required to switch to an active miR-222 state. By understanding this interaction, we can determine how dynamic ligand signaling and epigenetic feedback mechanisms cooperate to define stable cell states [42–44].

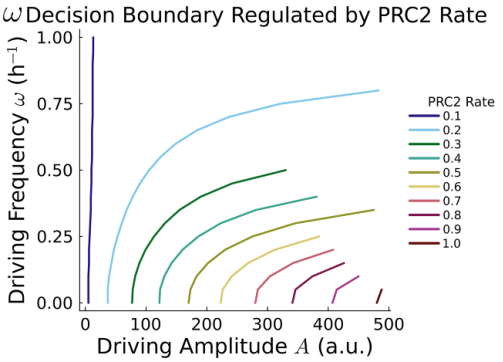

Figure 5. Modulation of the switching boundary by PRC2 feedback strength (p). The phase-independent A–ω boundary (for $\Delta T = 50$) shifts downwards and rightwards as p increases (from 0.1 to 1.0), indicating that stronger H27-state stabilization requires higher amplitude or lower frequency signals to induce switching regardless of initial phase. Units: A in a.u., ω in h^{-1}. Parameter p corresponds to PRC2 feedback strength.

3.3.2. PRC2 rate as a determinant of cellular decision boundaries

To further elucidate the role of PRC2 rate in cell fate decisions, we investigate how modulating PRC2 activity shifts the epigenetic decision boundary governing miR-222 activation. As displayed in figure 5, our simulations examine how PRC2 rate affects the amplitude–frequency ($A - \omega$) threshold, revealing its role as an epigenetic tuning parameter that controls the sensitivity of miR-222 to Notch signaling.

By increasing PRC2 rate (parameter p), we introduce stronger stabilization of the H27 state, necessitating higher NICD signaling level to overcome the repression and drive gene activation. This effect is particularly evident in the downward and rightward shift of the phase-independent A-ω boundary curve, which indicates that cells with a higher PRC2 rate require a greater Notch signal amplitude or lower frequency to transition to a stable H4-high state. These findings establish PRC2 rate as a critical epigenetic determinant that shapes the Notch-dependent decision boundary, ultimately influencing the stability of epigenetically controlled melanoma cell states.

3.4. Global sensitivity analysis identifies hierarchical control

The demethylation rate d provides the only substantial first-order contribution ($S_1(d) = 0.226$) because it directly counteracts methylation without feedback protection. Parameters embedded in feedback (m: NICD nuclear import, k: KDM5A demethylase, α_1: NICD-driven chromatin activation) exhibit negligible first-order effects but large total-order indices ($S_T(m) = 0.557$, $S_T(k) = 0.502$, $S_T(\alpha_1) = 0.429$), indicating that their influence arises through parameter combinations. Feedback coefficients pp and kk follow the same pattern ($S_1(pp) = 0.058$, $S_1(kk) \approx 0$, yet $S_T(pp) = 0.192$, $S_T(kk) = 0.046$) because they enter exclusively through the ratio $\Pi_4 = pp/kk$, so coordinated changes matter more than individual variations.

The threshold-independent Sobol analyses (final H4, H4 area-under-curve, and peak H4) exhibit interaction shares between 66% and 80%, matching the coupled Π-group structure where parameters enter multiple dimensionless ratios simultaneously. Across these metrics, the same chromatin-control parameters (m, d, α_1, k, p) dominate: α_1 provides the largest first-order contribution, m and d maintain the highest total-order indices, and p retains substantial total sensitivity despite its small independent effect because it operates through the chromatin ratios. The complete decompositions appear in SI section 3 (supplementary figure S1).

The sensitivity hierarchy directly reflects the mathematical structure revealed by dimensional analysis (SI section 3). Parameters m and d control the primary dimensionless groups Π_3 and Π_2 that determine bistability boundaries, explaining their large total-order indices. The substantial interaction effects (0.381 for m, 0.208 for d) arise from nonlinear coupling at the bifurcation: the critical value of one parameter depends on the other through the relation $\Pi_{4,\mathrm{crit}} = f(\Pi_2/\Pi_3)$ as derived in SI section 3. In contrast, feedback parameters pp and kk exhibit ratio protection—their individual variations cancel when both scale proportionally (since only $\Pi_4 = pp/kk$ enters the dynamics), providing robustness against correlated enzyme expression fluctuations common in biological systems. This hierarchical control architecture might be used to guide therapeutic targeting: perturbing PRC2/EZH2 shifts Π_3, modulating KDM5A alters Π_2, while interventions affecting KMT/KDM6A must be coordinated to displace Π_4 rather than merely rescale it.

3.5. Stochastic simulations capture population heterogeneity

Chemical Langevin simulations operate on the native copy numbers stored in the parameter database (tens to hundreds of chromatin-modifying enzymes), so no additional system-size rescaling is introduced. This keeps the model in a regime where intrinsic fluctuations remain appreciable while trajectories stay numerically stable.

Under identical pulsatile DLL1-like stimulation (amplitude 100, frequency $0.5\,h^{-1}$), individual cells exhibit highly variable switching trajectories: 67% complete the epigenetic transition from H4-high to H27-high chromatin states while 33% remain epithelial despite receiving the same signal (SI figure S8).

This incomplete penetrance arises from stochastic fluctuations in chromatin modification reactions: cells experiencing favorable fluctuations early in the signaling period accumulate H4 marks more rapidly and cross the switching threshold, while others fail to integrate sufficient signal before stimulation ends. The distribution of required pulses varies depending on frequency, with mean switching time of 12 h (coefficient of variation 0.27) under baseline conditions (SI section 6). These model predictions are qualitatively consistent with the partial EMT penetrance and heterogeneous timing observed in melanoma and other cancer cell populations [1, 19].

Critically, stochastic effects smooth the deterministic sawtooth patterns (visible in figure 4(b)) into continuous probability gradients. The sharp integer pulse requirements predicted by deterministic models become broad switching-time distributions in the intrinsic-noise regime, demonstrating that molecular noise is not merely a perturbation but a fundamental component of the EMT decision process. When we instead perturb the kinetic parameters themselves (log-normal $\sigma = 0.3$ Monte Carlo ensemble), only 37% of parameter draws complete the mesenchymal-to-epithelial transition, leaving a 63% non-switching reservoir even under identical signals. This partial response might help explain clinical experience with EZH2 inhibitors such as tazemetostat, which achieved objective response rates below 20% in solid-tumor cohorts despite target engagement [45], and with Notch-pathway inhibitors such as the γ-secretase inhibitor RO4929097, which produced disease stabilization but rare durable responses in melanoma patients [46]. These data lend support to dosing strategies that explicitly target the probabilistic non-switching subpopulation rather than assuming deterministic thresholds.

4. Discussion

We developed a mechanistic description of how dynamic Notch ligand codes are written into long-lived chromatin memory at the miR-222 locus. Motivated by observations that transient Notch activation can lock melanoma cells into an invasive state [10], the model links DLL1-like/DLL4-like-driven NICD trajectories to the coupled histone feedback loops that sustain or extinguish miR-222 expression [18].

Phenomenological modeling and dimensional analysis. A central methodological challenge is the absence of complete kinetic measurements for the 11 model parameters in melanoma EMT. Rather than attempting ill-posed parameter fitting to sparse endpoint data, we adopted a dimensional analysis approach (SI section 2) that reveals the system collapses onto three critical control groups: Π_2 (KDM5A-mediated demethylation), Π_3 (PRC2-mediated methylation), and Π_4 (feedback strength ratio). This reduction from 11 parameters to 3 dimensionless groups provides a rigorous mathematical framework for parameter selection while explicitly acknowledging data limitations. The approach yields testable scaling predictions and identifies which molecular processes control switching behavior independently of specific parameter values.

Epigenetic memory and dynamic signal interpretation. A central finding is the model's capacity for epigenetic memory through bistability. As demonstrated (figure 3), a sufficiently strong Notch signal, whether sustained or pulsatile, can induce a stable switch to the H4-high (active miR-222) state, which persists after signal withdrawal. This provides a mechanistic explanation for the lasting cellular changes observed following transient Notch signaling [10]. Furthermore, the model reveals how the epigenetic module processes dynamic signals, acting as a low-pass filter (figure 4). This frequency-dependent response means the system integrates signals over time and is less sensitive to high-frequency pulses compared to sustained or low-frequency inputs. This filtering property offers a mechanism for cells to interpret the distinct temporal dynamics generated by different Notch ligands (e.g. sustained DLL4-like vs. pulsatile DLL1-like signals [20, 21]). Such dynamic decoding could underlie the selective activation of downstream targets; for example, genes requiring prolonged signaling to overcome an epigenetic threshold might be preferentially activated by sustained DLL4-like signals, mirroring observations regarding Hes/Hey regulation [20].

Role of epigenetic feedback and crosstalk. The model's behavior hinges on the epigenetic feedback loops (table 1), where histone marks influence the enzymes that modify them [47, 48]. The interplay between activating (H3K4me3 via KMT/KDM6A) and repressive (H3K27me3 via PRC2/KDM5A) loops, coupled with the Notch-MR-KDM5A link [18], creates the bistable switch. The significance

of epigenetic regulation, including histone methylation and demethylation, in modulating Notch pathway output is well-established [41, 49–52]. Our model specifically highlights the role of PRC2, a key regulator of H3K27me3 [53, 54]. Modifying the PRC2 feedback strength alters the signaling threshold required for switching (figure 5), demonstrating how intrinsic epigenetic factors can tune cellular sensitivity to Notch input. This dynamic interplay between signaling and epigenetics is increasingly recognized as crucial in development and disease, including processes such as EMT [13, 55] and cell fate decisions [56, 57].

Dynamic ligand decoding. Phase-independent amplitude–frequency maps (figure 4) demonstrate that both DLL4-like sustained input and DLL1-like pulsatile input can trigger irreversible switching provided the signals integrate above a low-pass boundary. The switch counts pulses rather than simply tracking instantaneous amplitude, explaining why small timing differences between ligands translate into distinct epigenetic outcomes [20]. SI section 4 extends this analysis to exponentially decaying pulses, showing that biologically realistic waveform envelopes shift the boundary modestly ($\omega\tau \sim 1$) yet leave the qualitative filtering intact. Modulating PRC2 feedback redistributes the boundary (figure 5), illustrating how intrinsic chromatin states tune sensitivity to extracellular dynamics.

Hierarchies of chromatin control. Global Sobol analysis spanning 2600 simulations ranks NICD nuclear import (m) and receptor degradation (d) as the dominant control levers ($S_T > 0.48$), whereas the feedback pair (pp, kk) acts primarily through their ratio. Monte Carlo perturbations (37% switching under 30% log-normal noise; SI section 3) indicate that the canonical parameter set resides inside a broad operational wedge rather than on a knife edge. SI section 3 details the dimensionless validation and biological interpretation of this hierarchy, reinforcing how the Π-group structure explains both robustness and sensitivity. Together these results support experimental strategies that combine EZH2/KDM5 perturbations with optogenetic control of ligand frequency to test the predicted decision surface.

Numerical validation and comparative architecture. Solver cross-checks (Rosenbrock23, Tsit5, Rodas5P, TRBDF2) reproduce the deterministic 'wiggles' in the switching-time curves, confirming they arise from discrete pulse counting rather than numerical artifacts (SI section 5). Chemical Langevin simulations smooth that structure into broad outcome distributions (67% switching, with variable pulse requirements; SI section 6), aligning with partial EMT penetrance observed in heterogeneous melanoma cultures. The comparative analysis in SI section 7 demonstrates how the Notch module's bistable chromatin memory diverges from the NF-κB programme's graded enhancer priming [58]: both circuits decode temporal inputs through chromatin modifications, but only Notch exhibits bistability with persistent memory states, while NF-κB employs reversible, graded chromatin remodeling. This architectural difference reflects their distinct biological roles—irreversible developmental commitment (Notch) versus reversible adaptive responses (NF-κB).

Therapeutic implications and model generality. The model's prediction that epigenetic parameters tune sensitivity to Notch signals suggests therapeutic possibilities. EZH2, the catalytic subunit of PRC2, is a target in cancer therapy [59–61], with inhibitors under investigation in melanoma clinical trials [42, 62]. Our derived decision boundaries (figures 4 and 5) suggest that modulating EZH2/PRC2 activity could alter the cellular response threshold to oncogenic Notch signaling [16], potentially converting metastatic cells to a non-invasive state. The derived non-linear decision boundaries (figures 4 and 5) provide a quantitative framework for exploring such interventions. The underlying motif of a signaling pathway gating a bistable epigenetic switch may represent a general principle [63]. Similar concepts appear in NF-κB-driven epigenetic reprogramming [58] and drug resistance mechanisms [64]. Testable hypotheses arise from the model, such as how manipulating factors affecting ligand dynamics (e.g. glycosylation [65]) or chromatin accessibility (e.g. SWI/SNF activity [66]) might shift the predicted switching boundaries.

Experimental predictions

The model yields concrete, testable predictions that map to standard perturbations:

1. PRC2 inhibition experiments: EZH2 inhibitors should shift the A–ω boundary down/right, lowering the amplitude/frequency needed for switching; conversely, PRC2 upregulation should shift it up/left.
2. Modulating NICD turnover: altering receptor processing or degradation pathways should primarily affect switching along the frequency axis (effective ω), altering the low-pass cutoff.
3. Frequency-dependent response curves: engineering DLL1-like pulses versus DLL4-like sustained stimuli (sender cell choice or ligand constructs) while quantifying nuclear NICD, H3K27me3/H3K4me3 at the miR-222 locus, and miR-222 levels should recover the phase-independent thresholds we report.
4. Stochastic switching signatures: switching time distributions under fixed (A, ω) should be broad rather than deterministic, with incomplete

penetrance (partial switching) consistent with threshold-crossing under intrinsic noise. Using the native copy-number scale from the curated parameter set, our Chemical Langevin simulations predict 67% switching efficiency with coefficient of variation ∼0.27 in switching times; these stochastic signatures can guide calibration of effective noise levels against single-cell data.

5. Parameter estimation framework: fitting the model's A–ω boundary and ST–ω curves to time-course datasets (NICD, histone marks, and miR-222) provides a path to parameter estimation and prospective validation.

Limitations and future directions

While our model captures frequency-dependent chromatin switching through Notch signaling, several biological complexities remain beyond its current scope. First, the model focuses on histone modifications at the miR-222 locus without incorporating downstream targets such as MITF repression, ZEB1/2 activation, or the broader EMT transcriptional program. This simplification allows mathematical tractability but omits feedback loops that may stabilize or destabilize the metastatic phenotype. Second, we model idealized square-wave and exponential signals rather than the complex spatiotemporal patterns arising from cell–cell contact dynamics, lateral inhibition, and microenvironment heterogeneity observed in vivo.

Future extensions could address pathway crosstalk with TGF-β and Wnt signaling, which co-regulate EMT in melanoma. Incorporating these pathways would reveal how cells integrate multiple dynamic inputs to make fate decisions. The model could also benefit from explicit representation of cis-inhibition mechanisms [67] that shape Notch signal duration and amplitude at the single-cell level. Linking our predicted switching dynamics to single-cell RNA-seq trajectories [68] would validate whether the computed H4/H27 transitions correspond to observed EMT state distributions.

Finally, spatial effects such as cell–cell contact dynamics and tumor microenvironment heterogeneity represent important future directions. Extending the model to multicellular systems with spatially varying ligand fields could predict how tissue architecture influences metastatic conversion patterns. Such extensions would bridge from molecular mechanisms to tissue-level phenomena, providing a multiscale framework for understanding and potentially controlling melanoma progression.

Data availability statement

No new data were created or analysed in this study.

Acknowledgments

HL acknowledges the support of the NSF through the Center for Theoretical Biological Physics, Grant No. PHY-2019745 and through DMS-245957. EDS acknowledges the support of AFOSR through Grant FA9550-21-1-0289. TC and EDS acknowledge the support of NSF through Grant DMS-2052455.

Code availability

All simulation code and parameter databases are available at https://github.com/sontaglab/notch. The repository includes Julia scripts for ODE integration, parameter continuation analyses, and figure generation.

Conflict of interest

The authors declare no competing interests.

Author contributions

Tianchi Chen 0000-0001-6040-6537
Formal analysis (equal), Investigation (equal), Methodology (equal), Software (equal), Writing – original draft (equal), Writing – review & editing (equal)

M Ali Al-Radhawi 0000-0002-6761-4520
Formal analysis (equal), Investigation (equal), Methodology (equal), Writing – original draft (equal)

Herbert Levine 0000-0002-8819-9055
Conceptualization (equal), Project administration (equal), Supervision (equal), Writing – original draft (equal), Writing – review & editing (equal)

Eduardo D Sontag 0000-0001-8020-5783
Conceptualization (equal), Formal analysis (equal), Funding acquisition (equal), Investigation (equal), Project administration (equal), Supervision (equal), Writing – original draft (equal), Writing – review & editing (equal)

References

[1] Nieto M A, Huang R Y J, Jackson R A and Thiery J P 2016 The basics of epithelial-mesenchymal transition *Cell* **166** 21–45
[2] Yang J *et al* 2020 Guidelines and definitions for research on epithelial–mesenchymal transition *Nat. Rev. Mol. Cell Biol.* **21** 341–52
[3] Jolly M K, Ware K E, Xu S, Gilja S, Shetler S C, Wang N and Levine H 2017 EMT and MET: necessary or permissive for metastasis? *Mol. Oncol.* **11** 755–69
[4] Boareto M, Jolly M K, Goldman A, Pietilä M, Mani S A, Sengupta S, Ben-Jacob E, Levine H and Onuchic J'N 2016 Notch-Jagged signalling can give rise to clusters of cells

exhibiting a hybrid epithelial/mesenchymal phenotype *J. R. Soc. Interface* **13** 20151106
[5] Tang Y, Durand S, Dalle S and Caramel J 2020 EMT-inducing transcription factors, drivers of melanoma phenotype switching and resistance to treatment *Cancers* **12** 2154
[6] Artavanis-Tsakonas S, Rand M D and Lake R J 1999 Notch signaling: cell fate control and signal integration in development *Science* **284** 770–6
[7] Kopan R and Ilagan M X G 2009 The canonical Notch signaling pathway: unfolding the activation mechanism *Cell* **137** 216–33
[8] Henrique D and Schweisguth F 2019 Mechanisms of Notch signaling: a simple logic deployed in time and space *Development* **146** dev172148
[9] Schwanbeck R, Martini S, Bernoth K and Just U 2011 The Notch signaling pathway: molecular basis of cell context dependency *Eur. J. Cell Biol.* **90** 572–81
[10] Golan T *et al* 2015 Interactions of melanoma cells with distal keratinocytes trigger metastasis via Notch signaling inhibition of MITF *Mol. Cell* **59** 664–76
[11] Jia D, Jolly M K, Kulkarni P and Levine H 2017 Phenotypic plasticity and cell fate decisions in cancer: insights from dynamical systems theory *Cancers* **9** 70
[12] Chen T, Ali Al-Radhawi M and Sontag E D 2021 A mathematical model exhibiting the effect of DNA methylation on the stability boundary in cell-fate networks *Epigenetics* **16** 436–57
[13] Al-Radhawi M A, Tripathi S, Zhang Y, Sontag E D and Levine H 2022 Epigenetic factor competition reshapes the EMT landscape *Proc. Natl Acad. Sci.* **119** e2210844119
[14] Liu Y *et al* 2019 Competitive endogenous RNA is an intrinsic component of EMT regulatory circuits and modulates EMT *Nat. Commun.* **10** 1–12
[15] Liu X, Chen X, Yu X, Tao Y, Bode A M, Dong Z and Cao Y 2013 Regulation of microRNAs by epigenetics and their interplay involved in cancer *J. Exp. Clin. Cancer Res.* **32** 1–8
[16] Bhagat T D *et al* 2017 Notch pathway is activated via genetic and epigenetic alterations and is a therapeutic target in clear cell renal cancer *J. Biol. Chem.* **292** 837–46
[17] Liang Y-K *et al* 2018 MiR-221/222 promote epithelial-mesenchymal transition by targeting Notch3 in breast cancer cell lines *NPJ Breast Cancer* **4** 1–9
[18] Liefke R, Oswald F, Alvarado C, Ferres-Marco D, Mittler G, Rodriguez P, Dominguez M and Borggrefe T 2010 Histone demethylase KDM5A is an integral part of the core Notch–RBP-J repressor complex *Genes & Dev.* **24** 590–601
[19] Pastushenko I *et al* 2018 Identification of the tumour transition states occurring during EMT *Nature* **556** 463–8
[20] Nandagopal N, Santat L A, LeBon L, Sprinzak D, Bronner M E and Elowitz M B 2018 Dynamic ligand discrimination in the Notch signaling pathway *Cell* **172** 869–80
[21] Sprinzak D, Lakhanpal A, LeBon L, Santat L A, Fontes M E, Anderson G A, Mather W H and Elowitz M B 2010 Cis-interactions between Notch and Delta proteins generate mutually exclusive signalling states *Nature* **465** 86–90
[22] Fryer C J, White J B and Jones K A 2004 Mastermind recruits CycC: CDK8 to phosphorylate the Notch ICD and coordinate activation with turnover *Genes Dev.* **18** 2269–77
[23] Bray S J 2006 Notch signalling: a simple pathway becomes complex *Nat. Rev. Mol. Cell Biol.* **7** 678–89
[24] Al-Radhawi M A, Angeli D and Sontag E D 2020 A computational framework for a Lyapunov-enabled analysis of biochemical reaction networks *PLoS Comput. Biol.* **16** e1007681
[25] Wong B 2011 Points of view: color blindness *Nat. Methods* **8** 441
[26] Breiding P and Timme S 2018 HomotopyContinuation.jl: a package for homotopy continuation in Julia (available at: www.JuliaHomotopyContinuation.org)
[27] Dodd I B, Micheelsen M A, Sneppen K and Thon G'eve 2007 Theoretical analysis of epigenetic cell memory by nucleosome modification *Cell* **129** 813–22
[28] Sneppen K 2019 Models of life: epigenetics, diversity and cycles *Rep. Prog. Phys.* **82** 042601
[29] Tyson J J, Chen K C and Novak B 2003 Sniffers, buzzers, toggles and blinkers: dynamics of regulatory and signaling pathways in the cell *Curr. Opin. Cell Biol.* **15** 221–31
[30] Ferrell J E and Ha. S H 2014 Ultrasensitivity part III: cascades, bistable switches and oscillators *Trends Biochem. Sci.* **39** 612–8
[31] Voigt P, Tee W-W and Reinberg D 2013 A double take on bivalent promoters *Genes Dev.* **27** 1318–38
[32] Bintu L, Yong J, Antebi Y E, McCue K, Kazuki Y, Uno N, Oshimura M and Elowitz M B 2016 Dynamics of epigenetic regulation at the single-cell level *Science* **351** 720–4
[33] Gutenkunst R N, Waterfall J J, Casey F P, Brown K S, Myers C R and Sethna J P 2007 Universally sloppy parameter sensitivities in systems biology models *PLoS Comput. Biol.* **3** e189
[34] Saltelli A, Ratto M, Andres T, Campolongo F, Cariboni J, Gatelli D, Saisana M and Tarantola S 2008 *Global Sensitivity Analysis: The Primer* (Wiley)
[35] Rios A C, Serralbo O, Salgado D and Marcelle C 2011 Neural crest regulates myogenesis through the transient activation of Notch *Nature* **473** 532–5
[36] Mohtashami M, Shah D K, Nakase H, Kianizad K, Petrie H T and Zúñiga-Pflücker J C 2010 Direct comparison of DLL1-and DLL4-mediated Notch activation levels shows differential Lymphomyeloid lineage commitment outcomes *J. Immunol.* **185** 867–76
[37] Aymoz D, Solé C, Pierre J-J, Schmitt M, de Nadal E'alia, Posas F and Pelet S 2018 Timing of gene expression in a cell-fate decision system *Mol. Syst. Biol.* **14** e8024
[38] Ali Md Z and Brewster R C 2022 Controlling gene expression timing through gene regulatory architecture *PLoS Comput. Biol.* **18** e1009745
[39] Trapnell C, Cacchiarelli D, Grimsby J, Pokharel P, Li S, Morse M, Lennon N J, Livak K J, Mikkelsen T S and Rinn J L 2014 The dynamics and regulators of cell fate decisions are revealed by pseudotemporal ordering of single cells *Nat. Biotechnol.* **32** 381–6
[40] Yosef N and Regev A 2011 Impulse control: temporal dynamics in gene transcription *Cell* **144** 886–96
[41] Schwanbeck R 2015 The role of epigenetic mechanisms in Notch signaling during development *J. Cell. Physiol.* **230** 969–81
[42] Gallardo A *et al* 2022 EZH2 endorses cell plasticity to non-small cell lung cancer cells facilitating mesenchymal to epithelial transition and tumour colonization *Oncogene* **41** 3611–24
[43] DuPage M, Chopra G, Quiros J, Rosenthal W L, Morar M M, Holohan D, Zhang R, Turka L, Marson A and Bluestone J A 2015 The chromatin-modifying enzyme EZH2 is critical for the maintenance of regulatory T cell identity after activation *Immunity* **42** 227–38
[44] Moro A, Gao Z, Wang L, Yu A, Hsiung S, Ban Y, Yan A, Sologon C M, Chen X S and Malek T R 2022 Dynamic transcriptional activity and chromatin remodeling of regulatory T cells after varied duration of interleukin-2 receptor signaling *Nat. Immunol.* **23** 802–13
[45] Italiano A *et al* 2018 Tazemetostat, an EZH2 inhibitor, in relapsed or refractory B-cell non-Hodgkin lymphoma and advanced solid tumours: a first-in-human, open-label, phase 1 study *Lancet Oncol.* **19** 649–59
[46] Tolcher A W *et al* 2012 Phase I study of ro4929097, a gamma secretase inhibitor of Notch signaling, in patients with refractory metastatic or locally advanced solid tumors *J. Clin. Oncol.* **30** 2348–53
[47] Mukhopadhyay S and Sengupta A M 2013 The role of multiple marks in epigenetic silencing and the emergence of a stable bivalent chromatin state *PLoS Comput. Biol.* **9** e1003121
[48] Ku W L, Girvan M, Yuan G-C, Sorrentino F and Ott E 2013 Modeling the dynamics of bivalent histone modifications *PLoS One* **8** e77944

[49] Borggrefe T and Liefke R 2012 Fine-tuning of the intracellular canonical Notch signaling pathway *Cell Cycle* **11** 264–76
[50] Antfolk D, Antila C, Kemppainen K, Landor S K-J and Sahlgren C 2019 Decoding the PTM-switchboard of Notch *BBA-Mol. Cell Res.* **1866** 118507
[51] Wei C, Phang C-W and Jiao R 2020 Epigenetic regulation of Notch signaling during *Drosophila* development *Notch Signaling in Embryology and Cancer* (Springer) pp 59–75
[52] Oswald F *et al* 2016 A phospho-dependent mechanism involving NCoR and KMT2D controls a permissive chromatin state at Notch target genes *Nucleic Acids Res.* **44** 4703–20
[53] Seelk S, Adrian-Kalchhauser I, Hargitai B, Hajduskova M, Gutnik S, Tursun B and Ciosk R 2016 Increasing Notch signaling antagonizes PRC2-mediated silencing to promote reprograming of germ cells into neurons *eLife* **5** e15477
[54] Han X *et al* 2017 Notch represses transcription by PRC2 recruitment to the ternary complex *Mol. Cancer Res.* **15** 1173–83
[55] Serrano-Gomez S J, Maziveyi M and Alahari S K 2016 Regulation of epithelial-mesenchymal transition through epigenetic and post-translational modifications *Mol. Cancer* **15** 1–14
[56] Felician G, Collesi C, Lusic M, Martinelli V, Ferro M D, Zentilin L, Zacchigna S and Giacca M 2014 Epigenetic modification at Notch responsive promoters blunts efficacy of inducing Notch pathway reactivation after myocardial infarction *Circ. Res.* **115** 636–49
[57] Katakia Y T *et al* 2022 Dynamic alterations of H3K4me3 and H3K27me3 at ADAM17 and Jagged-1 gene promoters cause an inflammatory switch of endothelial cells *J. Cell. Physiol.* **237** 992–1012
[58] Cheng Q J, Ohta S, Sheu K M, Spreafico R, Adelaja A, Taylor B and Hoffmann A 2021 NF-κB dynamics determine the stimulus specificity of epigenomic reprogramming in macrophages *Science* **372** 1349–53
[59] Liao Y *et al* 2022 Inhibition of EZH2 transactivation function sensitizes solid tumors to genotoxic stress *Proc. Natl Acad. Sci.* **119** e2114965119
[60] Mirzaei S *et al* 2022 The long and short non-coding RNAs modulating EZH2 signaling in cancer *J. Hematol. Oncol.* **15** 1–34
[61] Zhang Y *et al* 2022 Genome-wide CRISPR screen identifies PRC2 and KMT2D-COMPASS as regulators of distinct EMT trajectories that contribute differentially to metastasis *Nat. Cell Biol.* **24** 554–64
[62] Zhdanovskaya N, Firrincieli M, Lazzari S, Pace E, Rossi P S, Felli M P, Talora C, Screpanti I and Palermo R 2021 Targeting Notch to maximize chemotherapeutic benefits: rationale, advanced strategies and future perspectives *Cancers* **13** 5106
[63] Siegal-Gaskins D, Mejia-Guerra M K, Smith G D and Grotewold E 2011 Emergence of switch-like behavior in a large family of simple biochemical networks *PLoS Comput. Biol.* **7** e1002039
[64] Su Y *et al* 2019 Kinetic inference resolves epigenetic mechanism of drug resistance in melanoma *bioRxiv Preprint* 724740
[65] Rana N A and Haltiwanger R S 2011 Fringe benefits: functional and structural impacts of o-glycosylation on the extracellular domain of Notch receptors *Curr. Opin. Struct. Biol.* **21** 583–9
[66] Pillidge Z and Bray S J 2019 SWI/SNF chromatin remodeling controls Notch-responsive enhancer accessibility *EMBO Rep.* **20** e46944
[67] Nandagopal N, Santat L A and Elowitz M B 2019 Cis-activation in the Notch signaling pathway *eLife* **8** e40541
[68] Zhang J, Nie Q and Zhou T 2019 Revealing dynamic mechanisms of cell fate decisions from single-cell transcriptomic data *Front. Genet.* **10** 1280